

Analyzing the Performance of a Nanosatellite Cluster-Detector Array Receiver for Laser Communication

Denis Bushuev, Debbie Kedar, *Student Member, IEEE*, and Shlomi Arnon, *Senior Member, IEEE*

Abstract—This work analyzes laser communication between a cluster of nanosatellites, which is a concentrated formation of small lightweight satellites and a ground station. The scenario under consideration is a cluster of nanosatellites communicating by means of a laser beam with a detector array receiver that is located on the earth's surface and equipped with a common optical system for all incoming beams. The beams are concentrated to spots over the detector plane by the receiver's optics. The detector array enables the ground station to communicate with a tight concentration of the nanosatellites, which reduces system complexity and cost. A critical parameter that determines the successful receipt and subsequent decoding of a transmitted signal for a given configuration is the angular separation between the satellites within the cluster. This separation must be retained to prevent critical overlapping of the spots on the detector's surface. The maximum allowable overlapping is calculated in terms of given bit-error rate. The spatial spreading of the beams, caused by scattering from aerosols in different layers of the atmosphere, is calculated for the case of single scattering. A stratified model of the atmosphere is used. Turbulence influences the beam width, especially for the case of short exposure, and is primarily caused by temperature changes, which result in fluctuations in the refractive index.

In this research, a new approach is adopted for analyzing communication network performance through the atmosphere by applying optical-transfer function (OTF) concepts used in imaging and remote sensing. We evaluate the effectiveness of this new approach in applications where spatial spread between the users is very important.

Index Terms—Detector arrays, laser communication, nanosatellites, optical transfer function.

I. INTRODUCTION

NANOSATELLITES are a promising solution for affordable laser space-space and laser space-ground communications [1]. The concept of a satellite cluster, distributed satellite system, or satellite flight formation has become very attractive for future missions in space for scientific research, for communication, for remote sensing, for synthetic aperture radar ([SAR], for example, Techsat21 [2]), and for navigation [3]. Clustering of a number of satellites enables the design of very small lightweight systems and reduces power requirements, fac-

Manuscript received May 2, 2002; revised September 19, 2002. This work was supported by the DIP Fund (Israeli-German research fund) and the donations of the OSLO Program by LAMBDA Research Optics, Inc., Littleton, MA 01460-4400 USA.

The authors are with the Satellite and Wireless Communication Laboratory, Electrical and Computer Engineering Department, Ben Gurion University of the Negev, IL-84105 Beer-Sheva, Israel (e-mail: bushuev@bgumail.bgu.ac.il; kedard@ee.bgu.ac.il; shlomi@ee.bgu.ac.il).

Digital Object Identifier 10.1109/JLT.2003.808770

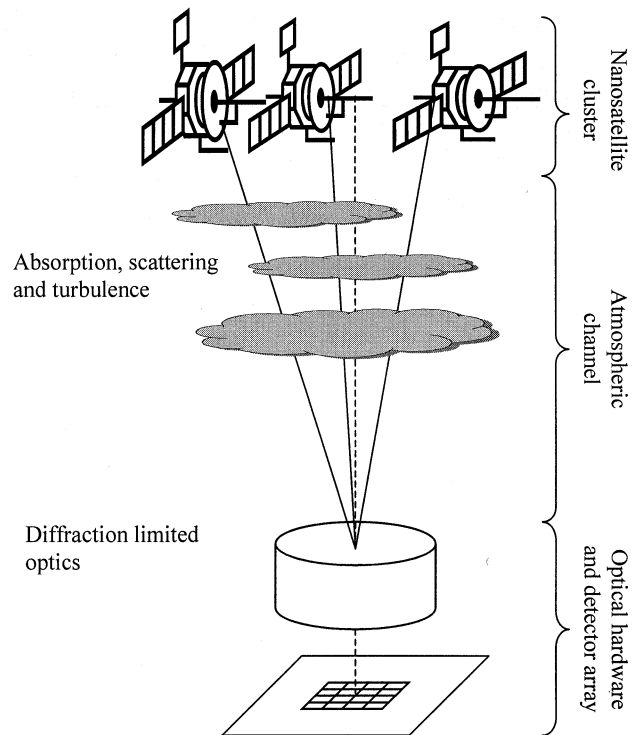


Fig. 1. Possible configuration for a nanosatellite cluster; earth downlink.

tors that make launching more affordable. The advantages of the laser intersatellite links are [1]: a) smaller size and weight of the terminal; b) less transmitter power; c) high immunity to interference; d) large data rate; and e) small transmitter-beam divergence angle. The same holds for communication to ground by nanosatellite, but the atmospheric effects such as aerosol scattering and turbulence must be considered and evaluated, as done in this paper. Fig. 1 demonstrates the nanosatellite cluster communicating with the ground station. While laser communication in space can transmit information over long distances without great distortion, the final stage presents problems. In the final stage, propagation takes place through the atmosphere (from the low orbit to ground station installation), where phenomena such as scattering and turbulence are encountered. This introduces serious distortions to the optical beam that decrease the received power, increase the bit-error rate (BER), and degrade the pointing efficiency [4]–[6]. Recently, appropriate system approaches have been investigated to contend with the growing need for practical design tools for optical-wireless communication networks [7], [8]. One approach to overcome the influence

of the atmosphere on laser beam propagation is the use of detector arrays instead of a single detector. This method enables the receiver to have a wider field of view (FOV) and also to control the noise power so as to decrease the BER [9]–[11]. Another significant advantage of the detector-array scheme is the ability to receive a number of different signals simultaneously.

In order to analyze the configuration illustrated in Fig. 1 from a practical point of view, one has to consider each satellite-earth downlink separately, with its own propagation-channel characteristics and signal distortions. For a large number of links, this technique considerably complicates the analysis of the system's performance. Instead, we suggest a novel "systems approach" for optical space and terrestrial communication analysis, which makes it possible to analyze the communication performance for a number of links simultaneously. The approach is based on concepts borrowed from imaging and remote sensing. These concepts involve the use of the optical-transfer function (OTF), which describes the object in terms of spatial frequencies. Much analytical and theoretical work has been done in these fields. We use some of the models that were developed to characterize the atmospheric channel and any given general configuration of an optical-communication system. The calculation of the minimal angular separation between satellites in a nanosatellite cluster was chosen as an appropriate trial example of the use of the imaging approach within the communication sphere. The critical angle was determined according to communication performance parameters of the main signal (such as BER) for a specific detector array.

The paper proceeds as follows. Section II consists of graphical and environmental descriptions of the communication system. Section III discusses the concept of the OTF and calculates it for optical hardware. Section IV presents mathematical analyses for the communication channel (atmosphere). Section V comprises the mathematical analyses for receiver performance. In Section VI, we describe the numerical calculation and present our results. Finally, we give brief conclusions.

II. THE SCENARIO

The scenario described in this work is presented in Fig. 1. The drawing shows that the communication system is made up of three key components. The first is a nanosatellite cluster, which is a group of small satellites located on the earth's low orbit at an elevation of approximately 800 km. Each nanosatellite is equipped with a laser and a transmitting telescope, which, for the sake of simplicity, are assumed to be identical in each unit. The system of data coding is simple ON-OFF keying (OOK), which operates in the C_β band of the wavelength-division multiplexing (WDM) standard at wavelengths from $\lambda = 1530.72$ nm to $\lambda = 1569.72$ nm. Thus, according to the WDM international standard [12], the average number of satellites taking part in the communication scenario is in the order of tens.

The second key component is the earth's atmosphere. An atmospheric channel is one of most complicated and unpredictable channels in communication, even by comparison with cellular networks. The influence of certain factors such as turbulence, aerosol scattering, and absorption result in power

degradation and spatial and temporal distortions in the received signal. In some cases, it may cause a serious increase in BER, and consequently, a complete link cutoff. In our scenario, the atmospheric model is layered. This means that the atmosphere is separated into different layers, each with its own intrinsic properties. In most cases of atmospheric channel analysis, it is appropriate to take into account a border layer located near the earth's surface whose depth is assumed to be approximately 2 km [13]. In this work, only the border layer is used.

The third component of the communication model has two parts: the first part is a receiver consisting optical hardware (lenses, polarizers, field stoppers, etc.) and the detector array, a matrix of tens of small low-noise photodiodes. This design is necessary for the reception of a large number of signals. Furthermore, it significantly reduces the need for precise pointing and yields a solution to the collection of power from a spatially dispersed signal without relinquishing the rapid time response. The second part is an electronic circuit for further signal processing.

III. OPTICAL-TRANSFER FUNCTION

Despite the basic coherent nature of laser radiation, the coherence length of most modern lasers does not exceed a few kilometers [14]. This theoretical coherence length may be an accurate description when propagating in a vacuum, but in the presence of various distortive media like fog, aerosols, and cloud formations, the actual coherence length is considerably less [15]. Therefore, we use a model of incoherent propagation. As a result of incoherent propagation, the characterization of light propagation is based upon a power-intensity distribution and not upon an electromagnetic field-amplitude distribution and hence, in this work, we employ the OTF and the point-spread function (PSF).

In electronics, the transfer function is defined as the Fourier transform (FT) of the impulse response. The OTF is defined similarly but is normalized to its own maximum value, which normally occurs at zero spatial frequency, as follows [14]:

$$\begin{aligned} \text{OTF} &= \tau(f) = \tau(f_x, f_y) \\ &= \frac{\int_{-\infty}^{\infty} \int_{-\infty}^{\infty} s(x', y') \exp[-j(f_x x' + f_y y')] dx' dy'}{\int_{-\infty}^{\infty} \int_{-\infty}^{\infty} s(x', y') dx' dy'} \\ &= \frac{S(f_x, f_y)}{S(0, 0)} = \text{MTF} \exp(j\text{PTF}) \end{aligned} \quad (1)$$

where $f = (f_x, f_y)$ is the spatial frequency in lines per meter and $S(f_x, f_y)$ is the FT of the PSF $s(x', y')$. According to (1), the OTF can be separated into two components: magnitude and phase. The magnitude component, known as the modulation-transfer function (MTF), is responsible for the form of the received signal in terms of spatial coordinates. The phase component, known as phase transfer function (PTF), is less important than the MTF, but often cannot be neglected. Spatial phase determines pulse position and orientation, rather than size.

Adopting the systems engineering approach and signal processing theory we can write

$$H_{\text{img}}(f_x, f_y) = \tau(f_x, f_y) H_{\text{obj}}(f_x, f_y), \quad (2)$$

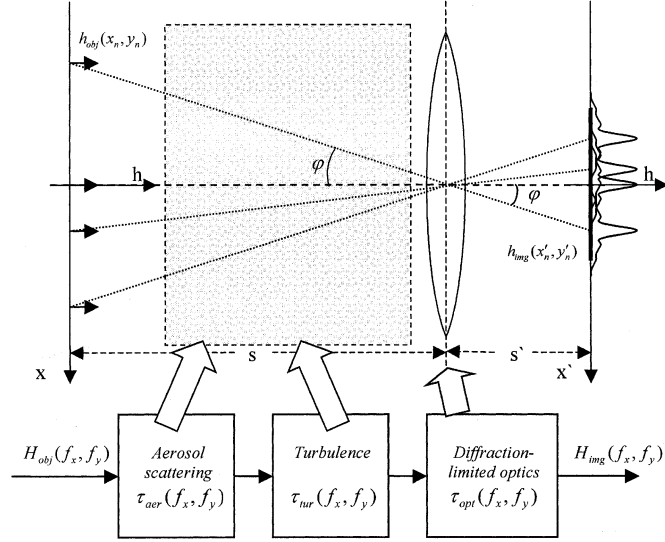


Fig. 2. Simple optical model with equivalent signal processing system demonstrating the propagation of an optical signal through the atmosphere and the receiver's optics.

where $H_{obj}(f_x, f_y)$ and $H_{img}(f_x, f_y)$ are intensities of the input and output signals in the spatial frequency domain and $\tau(f_x, f_y)$ is the system's OTF.

A. The System's OTF

Now, it is very straightforward to calculate the system OTF using the following components:

- 1) aerosol scattering OTF τ_{aer} ;
- 2) turbulence OTF τ_{tur} ;
- 3) optical hardware OTF τ_{opt}

This is formulated as

$$\tau(f_x, f_y) = \tau_{aer}(f_x, f_y)\tau_{tur}(f_x, f_y)\tau_{opt}(f_x, f_y). \quad (3)$$

Let us assume that each emitting element (transmitter) in the object plane within the nanosatellite cluster can be a spatial δ -function, positioned at different locations in x and y coordinates [15]. This situation is depicted in Fig. 2 and is formulated as

$$\begin{aligned} h_{obj}(x, y) &= h_1\delta(x - x_1, y - y_1) \\ &\quad + h_2\delta(x - x_2, y - y_2) + \dots \\ &= \sum_{n=1}^N h_n\delta(x - x_n, y - y_n). \end{aligned} \quad (4)$$

Here, N is the number of links participating in the communication scenario.

Also, for ease of calculation, we set the value of h_n to be equal to h_0 in all the transmitters. Hence,

$$h_{obj}(x, y) = h_0 \sum_{n=1}^N \delta(x - x_n, y - y_n). \quad (5)$$

Finally, in the spatial frequency domain, (5) can be rewritten as

$$H_{obj}(f_x, f_y) = h_0 \sum_{n=1}^N \exp(-j2\pi f_r r_n) \quad (6)$$

where

$$f_r = \sqrt{f_x^2 + f_y^2}, \quad r_n = \sqrt{x_n^2 + y_n^2}. \quad (7)$$

B. Diffraction-Limited Optics

The influence of optics on system performance has been widely discussed in research works in the fields of imaging and wireless optical communication. The main purpose of optical hardware is to receive and collect the incoming signal for which we need imaging optics to implement the multi-channel link. In this work, the diffraction-limited optics formulae refer to an equivalent lens of aperture diameter D and focal length f . The detector arrays are placed at the focus of the lens. The diffraction-limited optics OTF does not include the PTF component and, consequently, does not affect the position of the received signal. The MTF is given by [14]–[16], as in (8), shown at the bottom of the page, where

$$\alpha_0 = \frac{k_0 D}{2f}, \quad \omega = 2\pi f_r, \quad f_r = \sqrt{f_x^2 + f_y^2} \quad (8)$$

where D is the receiver-aperture diameter, f_r is the radial spatial frequency in cycles per meter, f is the focal length, and k_0 is the wavenumber.

IV. COMMUNICATION CHANNEL

In wireless communication, the channel is the atmosphere. Both spatial and temporal degradation of the signal in the atmospheric channel can be attributed to three main causes: absorption, aerosol scattering, and turbulence. These mechanisms can be considered independently, although some interaction is present.

A. Transmission

Absorption of radiation is a mechanism by which the atmosphere is heated. The infrared absorption by the atmosphere is due primarily to water vapor and CO_2 , with a smaller contribution from gases such as O_2 , N_2O , and CH_4 . The atmospheric

$$\tau_{opt}(\omega, \lambda) = \begin{cases} \frac{2}{\pi}, \left[\cos^{-1} \left(\frac{\omega}{2\alpha_0} \right) - \frac{\omega}{2\alpha_0} \sqrt{1 - \left(\frac{\omega}{2\alpha_0} \right)^2} \right] & \omega \leq 2\alpha_0 \\ 0, & \omega \geq 2\alpha_0 \end{cases} \quad (8)$$

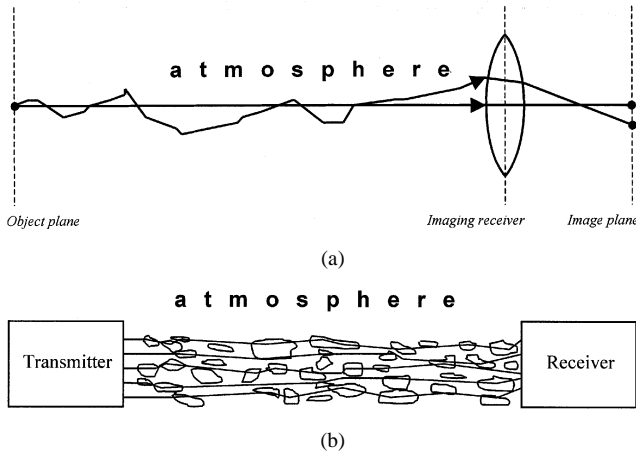


Fig. 3. (a) Unscattered radiation (straight line) and multiple forward-scattered radiation at two different locations in the image plane. (b) Distortions in the beam form caused by spontaneous fluctuations in the index of refraction during propagation.

absorption is very wavelength selective and contains a number of regions called “absorption windows” [13], in which absorption is minimal. Therefore, it is necessary to carefully choose the optical carrier frequency or carrier-frequency range to provide the required transmittance. For the near-infrared range, absorption windows exist at 1.5 to 1.7 μm and 2.0 to 2.5 μm . Those regions include the *C*, *L*, and *S*-bands of the WDM communication standard [12].

B. Aerosol Scattering

Scattering of photons by airborne particulates is manifested as deflections of the photons to directions other than that of their original propagation. If such scattering causes the deflected photons to miss the receiver, then the scattering results in attenuation. The received irradiance of the signals propagated through the atmosphere is correspondingly diminished from that in the object plane. However, if the light scattering is at very small angles with respect to the original directions of propagation, then forward-scattered radiation can take a roundabout path and still be received by the imaging system together with the unscattered radiation. This is illustrated in Fig. 3(a) for one multiple forward-scattered ray and one unscattered ray. Many such multiple-scattering paths give rise to a relatively large blurred-point images rather than a fine sharp-point image. The main scatterers in the earth’s atmosphere are molecules of air and aerosols.

The influence of air molecules and aerosol molecules on light propagation is described by the theories of Rayleigh and Mie, respectively [16]. In the case of Rayleigh scattering, much energy is lost, since the scattering is in all directions, including backward. Therefore, Rayleigh scattering is the primary attenuation mechanism. However, in the case of Mie scattering, much

light is forward-scattered at small angles, causing a blur in the receiver plane. Therefore, Mie scattering is considered the dominant mechanism in degrading imaging. Even in the situation of extremely clear air, a small amount of aerosols remain, whose scattering effects are much greater than those of molecular scattering with regard to image degradation [16]. Mie scattering theory makes it possible to find different parameters to characterize the scattering phenomena, such as the scattering and absorption coefficients S_a and A_a , which are used in the calculation of aerosol OTF.

Despite the blur produced by scattering, the aerosol scattering OTF does not affect the point position and thus contains only an MTF component and no PTF part. Hence, the MTF for aerosol scattering can be expressed as [16] as in (10), shown at the bottom of the page, where S_a and A_a are scattering and extinction coefficients respectively, f_a is the radial spatial frequency expressed in cycles per radian, L is the path length, and f_{ac} is the cutoff spatial frequency. The cutoff frequency f_{ac} is calculated according to the receiver’s characteristics, such as FOV, dynamic range and spatial bandwidth [16].

The aerosol scattering MTF for the short (10 ms) and long (1 s) exposures remains nearly equal [17]. Here, we assume that (10) is applicable for the case of a very small (10 ns) integration time such as that which also exists for optical-wireless communication. However, this assumption must be verified analytically and experimentally, and is not within the scope of this paper.

Conventional layer models consist of the following [16]: a boundary layer that ranges from 0 to 2 km, a region running from 2 to 6 km in which the number density displays an exponential decay with altitude (free troposphere), a stratospheric layer ranging from 6 to 30 km, and layers above 30 km composed mainly of particles that are extraterrestrial in origin. Note that from 15 to 25 km altitudes, there is usually an increase in aerosol light scatter caused by meteoric dust.

The average thickness of the aerosol-mixing region is approximately 2 km. This is the boundary layer. Within this region, one would expect the aerosol concentration to be influenced strongly by conditions at ground level. Consequently, aerosols in this region display the highest variability in meteorological conditions, climate, etc. Generally, aerosol size distribution hardly decreases with height, up to the boundary layer. Therefore, in practice, it is simple to describe this region as the main source of aerosol scattering that causes signal spatial distortion.

C. Turbulence

Variations in the index of refraction are the result of nonhomogeneities in the atmosphere. Nonhomogeneities are caused by thermal variations, which result from heat transfer between the earth and air. The variations are set in motion and mixed by wind and mechanical turbulence of airflow over terrain. The

$$\text{MTF}_{\text{aer}}(f_a) = \begin{cases} \exp\left\{-S_a L \left(\frac{f_a}{f_{ac}}\right)^2\right\} \bullet \exp\left\{\left[\frac{\exp\left\{-S_a L \left[1 - \left(\frac{f_a}{f_{ac}}\right)^2\right]\right\}}{-\exp(-S_a L)}\right] (-A_a L)\right\} & f_a < f_{ac} \\ \exp(-S_a L) \exp\{[1 - \exp(S_a L)] - A_a L\} & f_a \geq f_{ac} \end{cases} \quad (10)$$

propagation of the beam through zones of different refractive indices can be described with the help of Fig. 3(b). Here we see zones of inhomogeneities with different indices of refraction, but in contrast to the scattering case, here, the entire beam is distorted and there is no equivalent to the unscattered ray. The index of refraction variations in the atmosphere are described by the refractive-index structure parameter C_n^2 . Several models [18], [19] exist for estimating C_n^2 , all of which are dependent upon environmental and weather conditions. A critical factor in evaluating turbulence effects is the time scale of the exposure and the integration time of the detector (turbulence variation occurs at the rate of kHz). The OTF associated with turbulence can be described by either a long or short exposure model. The long exposure model integrates all the temporal variations in the vicinity of the blur in the focal plane. Thus, the turbulence OTF represents the spatial spread of the signal ray averaged over time, which determines power spread over the detector. Consequently, the PSF for long exposure will be wider and lower than that for short integration time.

As with the aerosol scattering OTF, in the long-exposure turbulence model, the position of a point ultimately does not alter. Hence, the turbulence OTF does not include a phase component. Therefore, only the MTF component exists and is expressed by [16]

$$\text{MTF}_{\text{tur},L}(f_a) = \exp \left[-57.53 a f_a^{5/3} \lambda^{-1/3} C_n^2 L \right] \quad (11)$$

where a is a wave-shape constant of 3/8 for spherical waves and 1 for planar waves. C_n^2 is the refractive-index structure parameter, λ is the wavelength, and L is the path length. For the vertical or slant path the spherical wave model is applied [16], because it better characterizes changes in refractive-index structure parameter C_n^2 with an altitude. The plane wave is an approximation of the spherical wave model and is applied in the case of weak changes in C_n^2 [16].

For short exposures of less than 10 ms [16], the transfer function is

$$\text{MTF}_{\text{tur},S}(f_a) = \text{MTF}_{\text{tur},L}(f_a) \exp \left[1 - \frac{1}{b} \left(\frac{f_a \lambda}{D} \right)^{1/3} \right] \quad (12)$$

where D is the receiver-aperture diameter (in units of wavelength) and $b = 2$ in the far field and 1 in the near field. Equations (11) and (12) were developed in the 1960s by Stanley [20] and recently, were experimentally verified by Sadot *et al.* [4].

The detector integration times for optical-wireless communication are in the order of nanoseconds and less. Hence, we use (12) to find turbulence OTF. We assume that (12) satisfies very short integration time, but this assumption must be investigated experimentally and analytically in future research works.

V. RECEIVER PERFORMANCE

Fig. 4 is a schematic illustration of the receiver. After calculation of the system's OTF $\tau(f_x, f_y)$, using (3), we compute the PSF, which indicates the system's transference of intensity. The PSF can be found by implementing the inverse FT of the system's OTF

$$i(x', y') = F^{-1} \{ \tau(f_x, f_y, \lambda) \}. \quad (13)$$

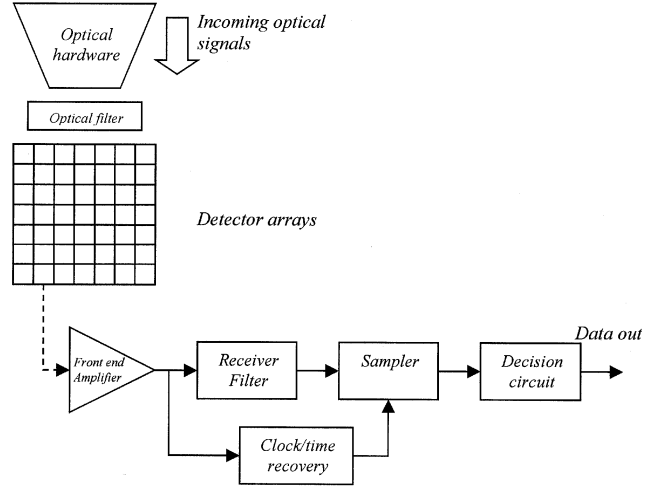


Fig. 4. Detector-array receiver.

The aerosol scattering, the turbulence, and the diffraction-limited optics do not produce any phase component in the system's OTF. The position of the received signals is defined by a spatial shift. The shift is determined by the spatial locations of the sources in the object plane, which is the system input. Therefore, we can easily summarize all outlet signals as follows:

$$I(x', y') = \sum_{n=1}^N i_n(x' - x'_n, y' - y'_n) \quad (14)$$

where (Fig. 2)

$$x'_n = \frac{f}{Z} x_n \quad (15)$$

and Z is the distance to the nanosatellite cluster from the receiving ground station.

To obtain the received-transfer power in the i, j coordinates, we have to find the transfer element $p_{i,j}$ given by

$$p_{i,j,n} = \int_{(i-1/2)d}^{(i+1/2)d} \int_{(j-1/2)d}^{(j+1/2)d} i_n(x' - x'_n, y' - y'_n) dx' dy' \quad (16)$$

where d is the size of a one-pixel detector.

The expression for h_0 in (5) can be written as the product of the following elements:

$$h_0 = P_T G_T L_T \quad (17)$$

where P_T , G_T , and L_T are transmitter power, gain, and loss, respectively. Once again, these are identical in each unit in the nanosatellite cluster configuration.

Overall received power is given by

$$\begin{aligned} P_{i,j} &= L_{FS} L_R G_R h_0 \sum_{n=1}^N p_{i,j,n} \\ &= L_{FS} L_R L_T G_R G_T P_T \sum_{n=1}^N p_{i,j,n}. \end{aligned} \quad (18)$$

where L_{FS} is the free space loss and L_R and G_R are the receiver loss and gain, respectively. The expressions for these elements can be found in [21].

We assume that one of the signals hits a given matrix element numbered i, j . In other words, this element is the main recipient for one communication link. Other signals can be considered as overlapping signals.

The received-current signal is given by

$$S_{i,j} = \Re P_{i,j} = S_{i,j,0} + S_{i,j,\text{ovr}} \quad (19)$$

where

$$S_{i,j,\text{ovr}} = \Re L_{\text{FS}} L_{\text{R}} L_{\text{T}} G_{\text{T}} G_{\text{R}} P_{\text{T}} \sum_{n=1}^{N-1} p_{i,j,n} \quad (20)$$

The coefficient \Re is the responsivity of the detector and is given by

$$\Re = \frac{\eta q}{h\nu} \quad (21)$$

where q is the electron charge, h is Plank's constant, ν is the optical radiation frequency, and η is the quantum efficiency.

A. Noise Statistics

In our model, we assume that all the detectors receive the same background radiation, which is a source of a background noise. The background noise can be expressed by [22]

$$\sigma_{\text{BG}}^2 = \frac{2q}{L^2} \Re \cdot N_{\text{BG}} \cdot \Delta\lambda \cdot \Omega \frac{D^2}{4} \pi \cdot B \quad (22)$$

where $\Delta\lambda$ is the filter bandwidth in micrometers, Ω is the receiver FOV, L is the number of detection-matrix elements (pixels) per row or column, D is the receiver-aperture diameter (in units of wavelength), B is the electronic bandwidth, and N_{BG} is the background spectral radiance in units of $\text{W}/(\text{m}^2 \text{ sr } \mu\text{m})$. In our paper, the sky is the main source of the background radiation.

The dark-current noise is given by [23]

$$\sigma_{\text{DC}}^2 = 2q I_{\text{DC}} B \quad (23)$$

where I_{DC} is the detector dark current.

The thermal noise is given by [23]

$$\sigma_{\text{TH}}^2 = \frac{4kT_e F B}{R_L} \quad (24)$$

where k is Boltzman's constant, R_L is the load resistance, F is the noise figure of the system, and T_e is the equivalent temperature.

From (22)–(24), the noise without any signal is given by

$$\sigma^2 = \sigma_{\text{TH}}^2 + \sigma_{\text{DC}}^2 + \sigma_{\text{BG}}^2. \quad (25)$$

In addition to the signal-independent noise sources described earlier in (22)–(24), there also exist shot and RIN noises. These are dependent upon the signal current and must be calculated for both the main and overlapping signals. Furthermore, in the case of overlapping signals, the RIN and shot-noise components must be calculated for each one of the disturbing signals separately. However, in most cases of free-space optic communication, the signal-shot and RIN noises are negligible in comparison to the background, Johnson, and dark-current noises [7]. Hence, the signal at the output of the detector can be written as

$$i_{i,j} = S_{i,j,0} + S_{i,j,\text{ovr}} + i_{\text{DC}} + i_{\text{BG}} + n_{i,j} \quad (26)$$

where $S_{i,j,0}$ is the main signal, $S_{i,j,\text{ovr}}$ is the sum of all overlapping signals, $n_{i,j}$ is the noise current (zero average), i_{DC} is the dark current, and i_{BG} is the background current.

After subtracting the direct-current components, we write

$$i_{i,j} = S_{i,j,0} + S_{i,j,\text{ovr}} + n_{i,j}. \quad (27)$$

B. BER Calculation

According to (27), the received signal comprises the main signal with the addition of two noise components. The $n_{i,j}$ term has a Gaussian-distribution form that facilitates calculations. However, the $S_{i,j,\text{ovr}}$ term includes beat noise, which is not described by Gaussian statistics. For further characterization of the system performance, we make some assumptions. First, the separation between the main signal and the overlapping one can be assumed to be equal for all distorting components. Second, once the overlapping channels are free of the signal-dependent noises, the probability of a simultaneous “one” for N overlapping signals can be calculated as the weighted sum of all the components. That is, [24]

$$p(q) = \frac{N!}{(N-q)!q!2^N} \equiv \frac{1}{2^N} \binom{N}{q} \quad (28)$$

where q is the number of channels in logical state “one” and N is the total number of overlapping signals. The average beat-error rate for a given threshold I_D can be easily calculated as follows [24]:

$$\text{BER} = \sum_{q=0}^N \text{BER}(I_D, q) p(q). \quad (29)$$

The N overlapping sources are considered statistically independent. Moreover, since the bandwidth of the transmitted signal is smaller than the separation between the channels, using the terminology of optical networks, only the outband crosstalk (overlapping) must be investigated. Assuming equal noise variance σ for transmitted binary “1” and binary “0,” the average BER can be written as

$$\text{BER} = \left(\frac{1}{2}\right)^{N+2} \sum_{q=0}^N \binom{N}{q} \times \left[\text{erfc}\left(\frac{I_{1,q} - I_d}{\sigma\sqrt{2}}\right) + \text{erfc}\left(\frac{I_d - I_{0,q}}{\sigma\sqrt{2}}\right) \right] \quad (30)$$

where the complimentary error function [23] is defined as

$$\text{erfc}(x) = \frac{2}{\sqrt{\pi}} \int_x^\infty \exp(-y^2) dy \quad (31)$$

and

$$I_{1/0,q} = I_{1/0} + qI_{\text{ovr}} \quad (32)$$

where I_{ovr} is the current produced by one overlapping source in logical state “one.”

VI. NUMERICAL CALCULATIONS AND RESULTS

In our scenario, the elevation of the cluster is assumed to be 800 km (LEO). The system-performance parameters

TABLE I
THE PROPOSED SYSTEM'S CHARACTERISTICS AND ASSOCIATED LINK BUDGET

Parameter	Value	Notes	Link Budget
Link range	8×10^2 km	Low earth orbit	-
Data rate	5 Gbit/sec	-	-
BER	2×10^{-10}	For a single link detection	-
Transmitter power	50 mW	-	17.99 dBm
Transmitter losses	75% transmission	-	-1.25 dB
Transmitter gain	27.6 μ rad beamwidth	-	103.40 dB
Free space losses	-	-	-256.35 dB
Atmospheric losses	75% transmission	-	-1.25 dB
Background spectral radiance	$2 W / (m^2 sr \mu m)$	The sky (day)	-
Refractive index structure parameter C_n^2	5×10^{-15}	-	-
Aerosol scattering coefficient	$8.4 \times 10^{-4} m^{-1}$	-	-
Aerosol absorption coefficient	$1 \times 10^{-5} m^{-1}$	-	-
Scattering- and turbulence-induced losses	-	Dependent on receiver characteristics	-9.87 dB
Optical filter	70 nm	Centered on 1550 nm	-
Receiving optics gain	$D=0.4$ m	$F^\# = 2.75$	130.33 dB
Receiving optics losses	75% transmission	Diffraction-limited	-1.25 dB
Detector's dimensions	$128 \times 128 \times 50 \mu m$	PIN matrix	-
Quantum efficiency	0.7	-	-
Received optical signal			-18.28 dBm

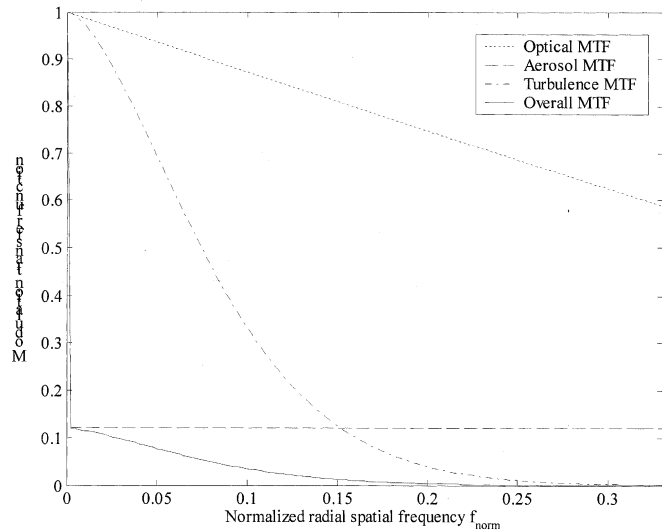


Fig. 5. Atmospheric and system MTFs: optical MTF (dotted line), turbulence MTF (dashed-dotted line), aerosol MTF (dashed line), and overall MTF (solid line).

are the data rate of 5 Gb/s, the optical wavelengths at the C-band (1530–1560 nm), and the optical power transmitted by each satellite, which is 50 mW. All the other parameters are described in detail in Table I. Two criteria influenced the choice of parameters: first, the low cost of the system was a priority, and this is embodied in the simplicity of the concept of the presented configuration. Second, the ease of maintenance of the communication link in the presence of problematical weather conditions such as fog and turbulence scintillations was considered. After determining the required parameters, the overall system OTF (MTF) was calculated (Fig. 5). The f_{norm} is given by

$$f_{\text{norm}} = \frac{2\pi f_r}{\alpha_0} \quad (33)$$

where α_0 and f_r are defined by (10).

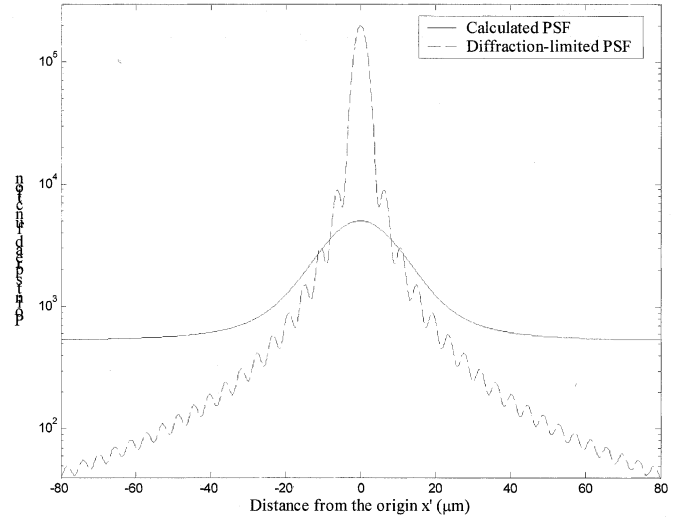


Fig. 6. Perfect (dashed line) and actual calculated (solid line) PSFs.

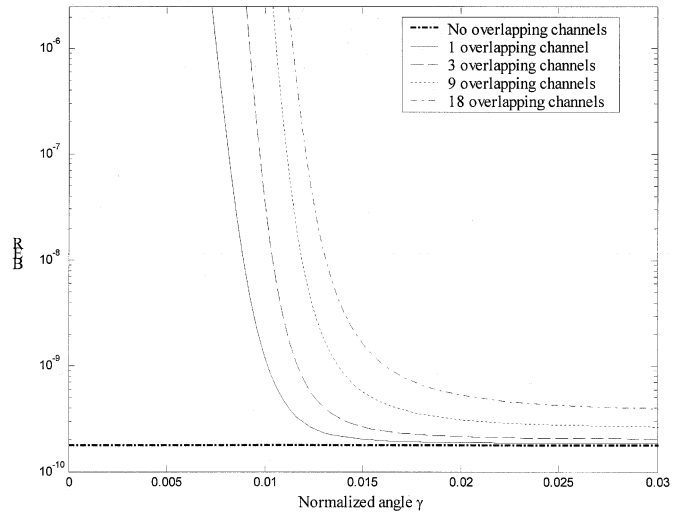


Fig. 7. BER versus the normalized separation angle between nanosatellites for 1 (solid line), 3 (dashed line), 9 (dotted line), and 18 (dashed-dotted line) overlapping channels. A single detection curve (bold, dashed-dotted line) demonstrates the minimal achievable BER.

As can be seen from the graph, the main distorting factor is the aerosol scattering. This causes the spread of energy over the detector array and consequent degradation of system performance. The turbulence also impacts the link budget. However, for a vertical propagation path, these effects are not extremely critical [16].

The PSF is depicted in Fig. 6. An undistorted or a so-called “perfect” point-spread function is also displayed. After the integration over the detector array element, the received signal was calculated and the BER in the presence of overlapping was evaluated (Fig. 7). The normalized angle is given by

$$\gamma = \frac{2\varphi}{FOV} \quad (34)$$

where φ is the separation angle. The BER for a single detection is presented as a reference curve. The BER evaluation was performed for a different number of overlapping channels. The figure shows that the BER curve sharply decreases as the angle increases. However, for a relatively large number of overlapping

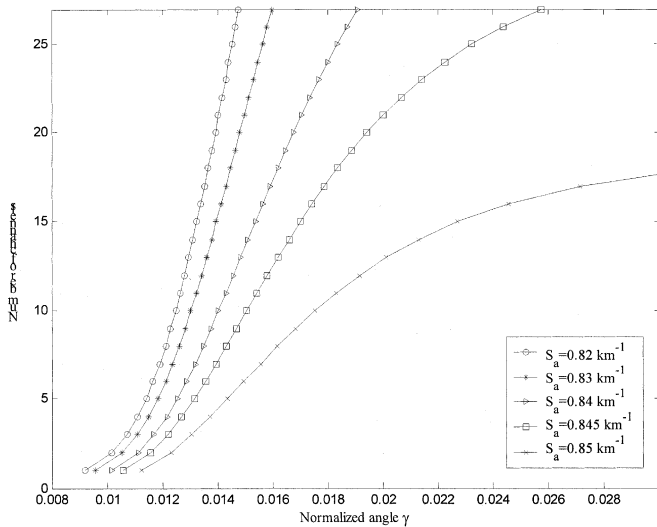


Fig. 8. Maximum number of channels versus the normalized separation angle between the nanosatellites for $\text{BER} = 10^{-9}$ with regard to different aerosol-scattering coefficients.

signals, the BER curve reaches saturation. This is caused by the very long “tails” of the calculated PSF, which extend far from the maximum intensity location.

In Fig. 8, we plot the maximum number of overlapping channels versus the separation angle γ for different scattering coefficients corresponding to various scattering conditions. The figure shows that as aerosol scattering increases, the performance degrades. The number of channels taking part in the link is limited even in the case of a very large separation (reversed slope of a curve for $S_a = 0.845 \text{ km}^{-1}$ and for $S_a = 0.85 \text{ km}^{-1}$).

VII. CONCLUSION

This paper describes optical communication through the atmosphere. We developed a novel approach to analyze laser-communication links in the presence of turbulence and aerosol scattering. The approach is based upon the OTF analysis of an optical signal’s power distribution. The calculation of BER was carried out for different separation angles for the case of multi-link atmospheric channels. Our main conclusion is that imaging techniques in general and OTF analysis in particular are applicable tools for characterizing the atmospheric optical channel. Another inference of this work is the high sensitivity of optical-wireless multilink communication to weather conditions and especially to aerosol-scattering phenomena. More detailed examination of the assumptions posed in this work for the case of aerosol scattering and turbulence is required to corroborate the theoretical work. Further application of the suggested analysis can lead to a better understanding of terrestrial wireless-optical multilink communication.

REFERENCES

- [1] R. W. Kaliski, S. M. Genco, D. Thompson, B. Breshears, T. O’Conner, K. M. Miller, E. W. Taylor, A. D. Sanchez, J. E. Winter, and R. Ewart, “Laser communication intersatellite links realized with commercial-off-the-shelf technology,” *Proc. SPIE*, vol. 3615, pp. 170–178, 1999.
- [2] H. Steyskal, J. K. Schindler, P. Franchi, and R. J. Mailloux, “Pattern synthesis for Techsat21—A distributed spacebased radar system,” in *Proc. IEEE Aerospace Conf.*, vol. 2, 2001, pp. 725–732.

- [3] G. Purcell, D. Kuang, S. Lichten, S.-C. Wu, and L. Young, “Autonomous formation flyer (AFF) sensor technology development,” *Telecommun. Mission Operation Prog. Rep. 42-134*, Jet Propulsion Lab., Pasadena, CA, 1998, [Online] Available: http://tmo.jpl.nasa.gov/tmo/progress_report/42-134/134J.pdf.
- [4] D. Sadot, D. Shemtov, and N. S. Kopeika, “Theoretical and experimental investigation of image quality through an inhomogeneous turbulent medium,” *Waves Random Media*, no. 4, pp. 177–189, 1994.
- [5] L. C. Andrews and R. L. Philips, *Laser Beam Propagation Through Random Media*. Bellingham, WA: SPIE, 1998.
- [6] S. Arnon, D. Sadot, and N. S. Kopeika, “Analysis of optical pulse distortion through clouds for satellite to earth adaptive optical communication,” *J. Modern Opt.*, vol. 41, no. 8, pp. 1591–1605, Aug. 1994.
- [7] X. Zhu and J. M. Kahn, “Free-space optical communication through atmospheric turbulence channels,” *IEEE Trans. Commun.*, vol. 50, pp. 1293–1300, Aug. 2002.
- [8] S. Arnon and S. Kopeika, “Effects of particulates on performance of optical communication in space and adaptive method to minimize such effects,” *Appl. Opt.*, vol. 33, no. 21, pp. 4930–4937, July 1994.
- [9] S. Arnon and N. S. Kopeika, “Free-space optical communication: Detector array aperture for optical communication through thin clouds,” *Opt. Eng.*, vol. 34, pp. 518–522, Feb. 1995.
- [10] E. Kayton, D. Marom, and S. Arnon, “A new approach to detector array receiver performance analysis for laser satellite communication, in free space laser communication and laser imaging,” *Proc. SPIE*, vol. 4489, pp. 118–125, 2001.
- [11] M. Srinivasan and V. Vilnrotter, “Avalanche photodiode arrays for optical communications receivers,” *Telecommun. Mission Operation Prog. Rep. 42-144*, Jet Propulsion Lab., Pasadena, CA, 2001, [Online] Available: http://tmo.jpl.nasa.gov/tmo/progress_report/42-144/144F.pdf.
- [12] R. Ramaswami and K. N. Sivarajan, *Optical Networks*. San Francisco, CA: Academic, 2002.
- [13] M. E. Thomas and D. D. Duncan, “Atmospheric transmission,” in *Atmospheric Propagation of Radiation*, F. F. Smith, Ed. Ann Arbor, MI: Environ. Res. Inst. Michigan, 1993.
- [14] C. S. Williams and O. A. Becklund, *Introduction to the Optical Transfer Function*. New York: Wiley, 1989.
- [15] R. Gagliardi and S. Karp, *Optical Communications*. New York: Wiley, 1995.
- [16] N. S. Kopeika, *A System Engineering Approach to Imaging*. Bellingham, WA: SPIE, 1998.
- [17] J. H. Richter and H. G. Hughes, “Marine atmospheric effects on electro-optical system performance,” *Opt. Eng.*, vol. 30, no. 11, pp. 1804–1820, Nov. 1991.
- [18] D. Sadot, S. Shamriz, I. Sasson, I. Dror, and N. S. Kopeika, “Prediction of overall atmospheric modulation transfer function with standard weather parameters: Comparison with measurements with two imaging system,” *Opt. Eng.*, vol. 34, no. 11, pp. 3239–3248, Nov. 1995.
- [19] I. Dror, S. A. S. Grossman, and N. S. Kopeika, “Accurate method for prediction of atmospheric transmission according to weather,” *Opt. Eng.*, vol. 35, no. 9, pp. 2548–2555, Sept. 1996.
- [20] R. E. Hufnagel and N. R. Stanley, “Modulation transfer function, associated with image transmission through turbulent media,” *J. Opt. Soc. Amer.*, vol. 54, pp. 52–61, Jan. 1964.
- [21] S. G. Lambert and W. L. Casey, *Laser Communications in Space*. Norwood, MA: Artech House, 1995.
- [22] S. Arnon, “Optical wireless communication,” in *The Encyclopedia of Optical Engineering (EOE)*. New York: Marcel–Dekker.
- [23] G. P. Agrawal, *Fiber-Optic Communication Systems*. New York: Wiley, 1997.
- [24] I. T. Monroy and E. Tangdiongga, “Performance evaluation of optical cross-connects by saddlepoint approximation,” *J. Lightwave Technol.*, vol. 16, pp. 317–323, Mar. 1998.

Denis Bushuev received the degree from Kemerovo State University, Kemerovo, Russia, in 1999. He is currently pursuing the M.Sc. degree in electrooptic engineering at Ben Gurion University of the Negev, Beer-Sheva, Israel.

His particular spheres of interest are optical wireless communication, atmospheric channel characterization, adaptive signal processing, and acousto-optic steering devices.

Debbie Kedar (S'02) received the M.A. degree in engineering science from Cambridge University, Cambridge, U.K., in 1982 and the M.Sc. degree from the Technion—Israel Institute of Technology, Haifa, Israel, in biomedical engineering in 1984. She is currently pursuing the Ph.D degree in the field of optical wireless communication at Ben Gurion University of the Negev (BGU), Beer-Sheva, Israel.

From 1984 to 1999, she worked as an Industrial Engineer in her home kibbutz. Recently, she has returned to retrain in electrooptic engineering at BGU. Her main research interests are in the fields of Monte Carlo simulation methods and the applications of communication in medicine.

Shlomi Arnon (SM'00) received the Ph.D. degree from Ben Gurion University, Beer-Sheva, Israel.

He was a Postdoctoral Associate (Fulbright Fellow) at the Laboratory for Information and Decision Systems (LIDS), Massachusetts Institute of Technology, Cambridge. He is currently a Faculty Member with the Electrical and Computer Engineering Department, BGU, and is the Founder of the Satellite and Wireless Communication Laboratory, which works intensively in the areas of laser satellite communication and terrestrial optical-wireless communication systems. He was invited and sponsored by the U.S. Air Force to consult with scientists in laboratories in Rome and Albuquerque, NM. He consults regularly with start-up and well-established companies in the area of optical-wireless communication and satellite communication. He delivered a workshop on laser satellite communication at NASA/JPL, Pasadena, CA. He co-instructed a tutorial on laser satellite communication at IEEE ICC 2000 in New Orleans, LA.

Dr. Arnon is the Israeli IEEE LEOS chapter Chair.